Graphical Abstract

Hey Ho, Where'd the Proton Go?; Final Deprotonation of O6 within the S$_3$ state of Photosystem II

Thomas Malcomson, Felix Rummel, Maxim Barchenko, Patrick O'Malley
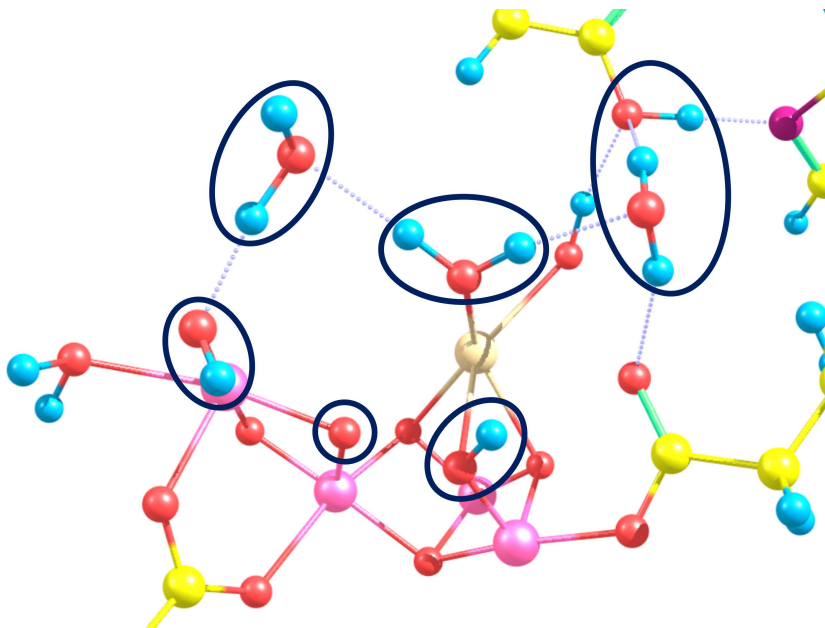
Highlights

Hey Ho, Where'd the Proton Go?; Final Deprotonation of O6 within the S$_3$ state of Photosystem II

Thomas Malcomson, Felix Rummel, Maxim Barchenko, Patrick O'Malley

- Data suggests final O6 deprotonation occurs via Ca bound W3 residue

- Stability of deprotonated structure is achieved at $\mathbf{r}$[O5O6] $\leq$ 2.0 Å

- High-spin state facilitates the necessary distribution of spin away from O6 required for stability

- Deprotonation via local Glu189 residue is highly unstable

- Final deprotonation of O6 corresponds to the formation of the first O5-O6 bond

Hey Ho, Where'd the Proton Go?; Final Deprotonation of O6 within the S_3 state of Photosystem II

Thomas Malcomson[a,*], Felix Rummel[b], Maxim Barchenko[b], Patrick O'Malley[b]

[a]School of Biosciences, Cardiff University, Museum Avenue, Cardiff, CF10 3AX, UK
[b]Department of Chemistry, School of Natural Sciences, The University of Manchester, Oxford Road, Manchester, M13 9PL, UK

Abstract

The deprotonation of O6 within the S_3 state marks the final deprotonation event before the formation of oxygen-oxygen bond interactions and eventual production and release of dioxygen. Gaining a thorough understanding of this event, from the proton acceptors involved, to the exfiltration pathways available, is key in determining the nature of the resulting oxygen species, influencing the mechanism through which the first oxygen-oxygen bond forms. Computational analysis, using BS-DFT methodologies, showed that proton abstraction by the local Glu189 residue provides consistent evidence against this being a viable mechanistic pathway due to the lack of a stable product structure. In contrast, abstraction via W3 shows an increasingly stable oxo-oxo product state between $\mathbf{r}[O5O6] = 2.1$ Å & 1.9 Å. The resulting oxo-oxo state is stabilised through donation of β electron character from O6 to Mn1 and α electron character from O6 to O5. This donation from the O6 lone pair is shown to be a key factor in stabilising the oxo-oxo state, in addition to showing the initiation of first O5-O6 bond.

*Keywords:* Photosystem II, BS-DFT, Oxygen Bond Formation, S_3 State

1. Introduction

Water oxidation in Photosystem II (PSII) is key to the presence of our aerobic atmosphere and as such understanding of catalytic cycle has been

---

*corresponding author
Email address: `malcomsont@cardiff.ac.uk` (Thomas Malcomson)

of great interest. At the heart of PSII is a $CaMn_4O_{5/6}$ complex, commonly referred to as the oxygen-evolving complex (OEC). Throughout the light driven water oxidation reaction two water molecules are consumed to produce molecular oxygen:

$$2H_2O \xrightarrow{4h\nu} O_2 + 4e^- + 4H^+ \tag{1}$$
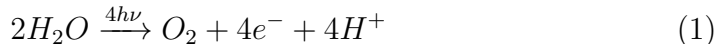
with this reaction proceeding in a step wise fashion as described by the Kok cycle[1]figure 1. Developing an in depth understanding of each event that occurs throughout nature's water oxidation reaction, with particular focus on the sequential deprotonation of each oxygen and the eventual formation of the dioxygen double bond, is key in the development of artificial water splitting complexes, which have direct applications in further addressing the global energy crisis.[2, 3, 4, 5]

It is necessary to remove 4 protons throughout the water oxidation reaction. Throughout the S_2 state, and subsequent transition to S_3, the second water molecule is inserted into the OEC and the first of its protons removed. This incoming water is generally thought to insert into the OEC in the "O6" position such that it is bound to Mn1 (figure 2). The general consensus as to the structure of the OEC at the initiation of the S_3 state is an O5 oxo-O6 hydroxo[6, 7, 8, 9], as shown in figure 2. Recent structural data suggests an O5-O6 distance of ≈ 2.0 Å[10, 11, 12], our group recently proposed that the presence of an equilibrium between this oxo-hydroxo starting structure and an oxo-oxo/$[O5O6]^{3-}$ intermediate structure within in the S_3 state is required to rationalise experimental electron paramagnetic resonance (EPR)
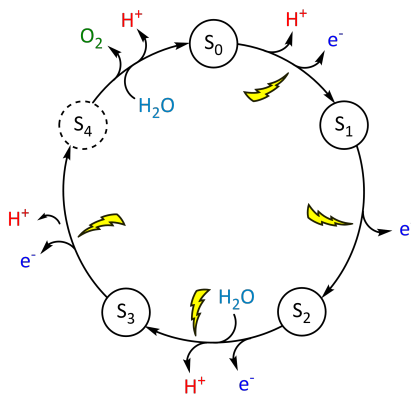

Figure 1: Summary of the Kok cycle, summarising the key steps for water oxidation.
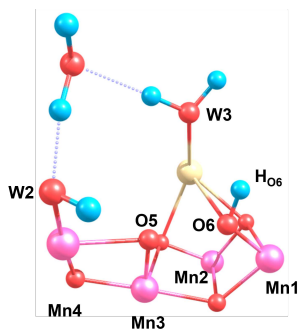
Figure 2: Summary of the Kok cycle, summarising the key steps for water oxidation.

data with higher accuracy that can be achieved with a pure oxo-hydroxo species.[13, 14]

There are many proposed O–O bond formation mechanisms, predominantly involving bond formation between O5 and O6.[15, 16, 17, 18, 19, 20, 21, 13, 14] Additionally, each of these mechanisms agree that, in order to move from an O5 oxo-O6 hydroxo species to molecular oxygen, a further proton must be removed from O6. In the recent PDB:7RF8 S_3 state crystal structure put forward by Hussein *et al*[22] two options present themselves based on the availability of proton acceptor species in the local environment: O6 can transfer its proton to the nearby Glu-189 residue, situated at a distance of 2.5 Å from O6; or the Ca bound W3, located 3.0 Å from O6 in the resolved crystal structure.

It has been suggested that protons lost from the OEC through the various deprotonation events exit the protein through the Cl1 channel which terminates close to the OEC Mn_4 bound W1 and W2 ligands.[23, 22] Understanding the proton release pathways for the various S state transitions would potentially give insights into the identity, and importance, of the substrate waters throughout the OEC.[24, 25] The proton transfer between W1 and Asp-61 has been investigated in more detail by several groups[26, 27, 28, 29, 30], and it has been suggested that the nature of the proton pathway between these two facilitates electron transfer from the OEC to the nearby Tyr-161 residue in the S_1 to S_2 transition, highlighting the importance of understanding proton transfer pathways to better rationalise the observed behaviour of the OEC.[28]

While the barrier for W1 to Asp-61 proton transfer is generally found to be low so far the O6 to Glu-189 barrier has been found to be significant

3

Table 1: Mulliken spin distributions of key centres within the OEC, across each broken-symmetry (BS) state presented, at the optimised oxo-hydroxo geometry, with a total system multiplicity of 13 such that $S_{\textbf{aaaa}} = 6$ and $S_{\textbf{baaa/aaba/aaab}} = 3$.

BS-State	Mn1	Mn2	Mn3	Mn4	O5	O6
aaaa	2.987	3.009	3.011	3.091	-0.104	0.047
baaa	-3.008	2.990	3.013	3.062	-0.095	-0.041
aaba	2.984	2.992	-2.931	2.995	-0.027	0.042
aaab	3.023	3.007	2.949	-2.974	0.035	0.057

with no stable minima located for a protonated Glu-189 in the S_2 state.[27] This study aims to investigate these potential deprotonation pathways in the S_3 state and presents potential energy surfaces for the deprotonation of O6 through abstraction by nearby W3 and Glu-189 moieties, and analysis of the relevant structures located on the PES to suggest a potential pathway for O6 deprotonation.

2. Methods

The methods used are similar to those described previously.[31, 32, 33] All calculations were performed in ORCA 4.2.1.[34] Models were initially optimised using the B3LYP functional[35, 36, 37, 38] in their high-spin (HS) oxidation states. The zeroth-order regular approximation (ZORA) Hamiltonian was applied to account for scalar relativistic effects[39, 40, 41] with the def2-SVP basis sets used for C and H atoms and the def2-TZVP basis set without f functions for all other atoms.[42]

For the systems presented here the B3LYP functional was chosen as it as a good track record for systems of this size and and for energetics and orbital analysis for the OEC[43] as well as other transition metal systems.[44] The chain of spheres (RIJCOSX) approximation was applied together with the decontracted general Weigend auxilary basis sets.[45, 46, 47, 48, 49] The conductor-like polarizable continuum model (CPCM) [50, 51] with a dielectric constant of $\epsilon = 8.0$ was used throughout to model the protein environment[52, 53], along with the Dispersion corrections proposed by Grimme with Becke-Johnson damping (D3BJ).[54, 55, 56, 57, 58] Tight SCF convergence criteria and increased integration grids (Grid6 and IntAcc 6 in ORCA convention) were used throughout, all terminal carbon atoms were

constrained during optimisations.

Initial BS-DFT wavefunctions were calculated using ZORA versions of the def2-TZVP with removed f functions for all atoms, and used for potential energy surface calculations.[42] The initial broken-symmetry (BS) guesses were obtained by use of the 'flipspin' feature of ORCA.[59] And convergence of the correct BS and HS states were confirmed by examination of the calculated Mulliken spin populations for all calculations.

All models were generated from the S_3 XFEL crystal structure (PDB: 7RF8)[22] and optimised with an assumed electronic configuration representative of the high-spin (HS) S_3 state with the O5-O6 distance constrained to 2.0 Å to maintain the separation observed in the crystal structure. Twelve directly coordinated amino acids are included in the models: Glu189, His-190 , Tyr-161 (Y_Z), Asp-342, His-332, Val-185, Glu-333, Glu-354, Asp-170, Ala-344, His-337, & Asp-61. Terminal carbon atoms were modelled as methyl groups (-CH_3) and constrained throughout all calculations.

Additionally, the peptide backbone linking Glu-189 and His-190 was included to assess the effect on Glu-189 orientation, R-groups along the chain were modelled as methyl (-CH_3) groups. The directly coordinated water molecules W1-W4 as well as two bridging and highly resolved crystallographic water molecules were also included. All oxygen bridges O1-O5 were in their fully deprotonated (O^{2-}) state, O6 was OH^- for the oxo-hydroxo models, and O^{2-} otherwise. W1, W3 and W4 were fully protonated, W2 was OH^- during the optimisation of the oxo-hydroxo starting model. Upon satisfactory optimisation of the HS-13 geometry, further optimisations were
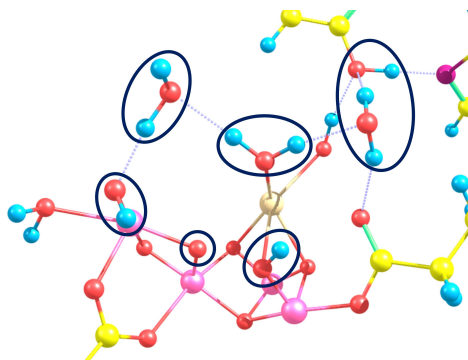

Figure 3: Schematic of oxo-hydroxo structure (additional amino acids removed for clarity), showing the residues left unconstrained (ovals) during the PES optimisations. Carbon = yellow; Oxygen = red; Hydrogen = blue; Manganese = magenta; Calcium = pale brown.

conducted with all atoms constrained, with only O5, O6, its corresponding hydrogen, W2, W3, the bridging waters, and the OH group of Yz free to move (figure 3). These constraints were deemed accessible through analysis of geometry variation both throughout the MnO complex and the surrounding amino acids, which was observed to be negligible throughout the O5-O6 arrangements studied (figure S1), in addition to the lack of expected change in geometry throughout the S3 state; in comparison to, as an example, the relative opening of the cubane structure observed in the S2 state, required to facilitate O6 insertion.[22]

Potential energy surfaces were generated utilising the same model chemistry as described above by scanning the $\mathbf{r}$[W3-H$_{O6}$] distance in 0.05 Å steps, with O5-O6 bond length varied between scans, where each point underwent optimisation in line with the above constraints to produce the final potential energy surface. Intrinsic bond orbitals (IBOs) were produced using IboView [60, 61] with iboexp=2 from the optimised PES wavefunctions.

Data is presented for four states in total, named in respect to the direction of the unpaired spin on each metal centre, these four states comprise of: a high spin state with a total multiplicity of 13 (S=6), **aaaa**, and three broken symmetry states involving the flipping of the spin on Mn1 (**baaa**), Mn3 (**aaba**), and Mn4 (**aaab**), such that the final spin multiplicity of the complex was 7 (S=3).

For clarity, Mulliken spin distributions, when reported, are presented as the deviation in the magnitude of spin on a given centre along the reaction surface from that of equivalent centre at the oxo-hydroxo geometry in a given electronic state, such that the spin (x) for the O6 centre is expressed as:

$$x^{O6}_{reported} = |x^{O6}|_{scan} - |x^{O6}|_{oxo-hydroxo} \qquad (2)$$

This has the benefit of presenting a sign-independent interpretation of the spin on a given centre, simplifying the need to account for the inverted spin in the **baaa**, **aaba**, and **aaab** states, such that a positive reported value signifies an increase in overall unpaired spin on a given centre, while a negative value should be interpreted as a reduction in overall unpaired spin (tending to zero) on the centre in question.

6

3. Results and Discussion

3.1. Abstraction by W3

Analysis of the O6-H_{O6} $\rightarrow$ W3 potential energy surface at an $\mathbf{r}$[O5O6] = 2.0 Å (figure 4), as found in the 7RF8 crystal structure, shows an **aaba** arrangement as the most stable in the oxo-hydroxo state, in line with previous calculations put forward,[33, 62, 31, 63, 32], however all broken-symmetry states are negligibly close in energy at this stage (within 1 $kcal\ mol^{-1}$). The difference in energy between the states is shown to steadily increase as the O6-H_{O6} bond is stretched and subsequently breaks, resulting in two clusters: **baaa** and **aaab** which are shown to be disfavoured by $\approx$3 $kcal\ mol^{-1}$; and **aaaa** and **aaba** at lower energies, with **aaaa** being shown to be the most stable at the oxo-oxo geometry. The **aaaa** state boasts a marginal 1 $kcal$ mol^{-1} stability over the **aaba** oxo-hydroxo geometry, providing a promising link with recent independent analysis of the oxo-hydroxo and oxo-oxo states.[33, 62, 31, 63, 32] The large drops in energy observed between 1.15 Å and 1.10 Å are attributed to the point at which the proximity of the O6 proton to W3 promotes subsequent and concerted proton transfer from W3 to the local crystallographic water, with a further proton exchange to W2. This transfer marks the dominant shift in the complex from an oxo-hydroxo electronic structure, to one resembling an oxo-oxo arrangement.

Subsequent analysis of the variation in spin on key atomic centres across the reaction coordinate for the **aaaa** state (figure 5; top) provides additional insight into the electronic movement within the system. The primary observed change is an increase in the spin on Mn4 (figure 5; yellow), which is more pronounced after the W2 protonation, and a decrease in the overall spin on Mn1 (figure 5; dark blue). Secondary changes are seen in the spin
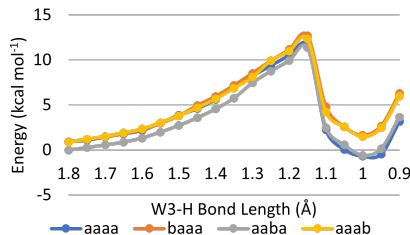

Figure 4: Energy profile of scan of increasing O6-H_{O6} distance, towards W3, at a fixed O5-O6 at $\mathbf{r}$[O5O6] = 2.0 Å.
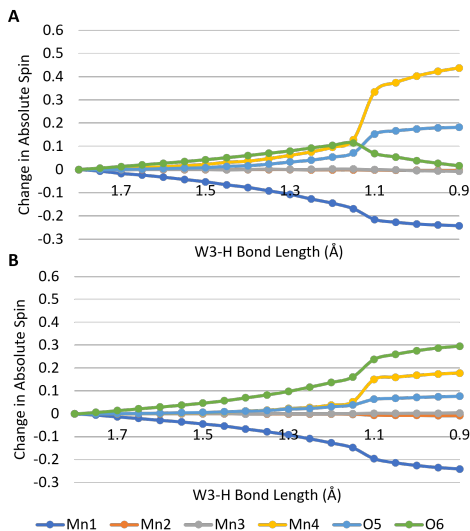
Figure 5: Change in absolute spin values of key atomic centres within the system during the oxo-hydroxo to oxo-oxo transition within the **aaaa** state (**A**) and **baaa** state (**B**) at **r**[O5O6] = 2.0 Å.

values of O5 and O6 (figure 5; light blue and green, respectively) in which O6 shows an initial gain in spin before a subsequent reduction between 1.15 Å and 1.10 Å, corresponding to a sharp increase in the spin of O5. While the increase in spin found on Mn4 is to be expected, the behaviour of Mn1, O5, & O6 are surprising.

Explanation of the unexpected spin behaviour can be found through consideration of key IBOs in both the oxo-hydroxo and oxo-oxo states (figure 6). While initial O6-H_{O6} bond stretch results in minor localisation of the O6 lone pair (LP) onto the oxygen centre, explaining the early increase in spin, transition to an oxo-oxo arrangement shows a separation in the O6 LP; movement of the β electron (figure 6; top) to the Mn1 centre accounts for the reduction in spin on Mn1 as the incoming β spin pairs with the existing α spin, while concerted movement of the corresponding α electron (figure 6; middle) towards O5 acts to explain the drop in spin on O6 at 1.15 Å, and the resulting increase on the O5 centre, in addition to signifying the initiation of O5-O6 bond formation. The expected increase in spin on the Mn4 centre is rationalised through the movement of an α electron from O5 (figure 6; bottom), this movement also accounts for the relatively small overall gain in

8

spin on O5; as α spin is donated from O6, concerted donation of α spin from O5 to Mn4, preventing a large accumulation of spin and, as a result, charge on the O5 centre.

Consideration of changes in the spin distribution, and equivalent IBOs also allow for insight into the difference in energy between the pairs of states shown in figure 4. While the **aaba** (figure S3; C) state shows a similar spin distribution to that of **aaaa**, **baaa** (figure 5; bottom) and **aaab** (figure S3; D) present a different distribution. Inversion of the spin on either the Mn1 or Mn4 centres acts to disrupt the dispersion of residual spin in the oxo-oxo form, post-O6-H$_{O6}$ bond breaking; in the presence of a spin-flipped Mn1 centre, it is an α electron from an O6 LP that now accounts for the decrease in overall spin on Mn1. This, coupled with the unperturbed movement of α spin from O6 to O5 and onward to Mn4, results in a much more significant build up of β spin on the O6 centre, leading to the disfavoured energetics relative to **aaaa**. The spin profile of **aaab** can be explain in an analogous manner, with β spin being pulled from the newly deprotonated O6 to both Mn1 and the spin-flipped Mn4, resulting in an equivalent accumulation of α spin on O6.
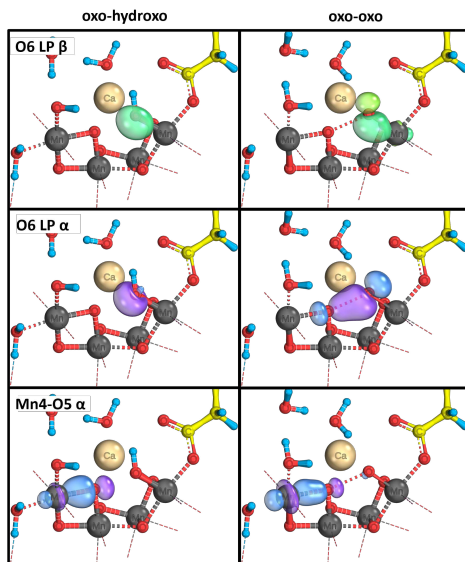

Figure 6: IBO representations of the orbitals showing the largest change during the transition between the oxo-hydroxo (left) and oxo-oxo (right) structures in the **aaaa** state, at $\mathbf{r}$[O5O6] = 2.0 Å, with regards the electronic character of O5, O6, and the Mn centres.
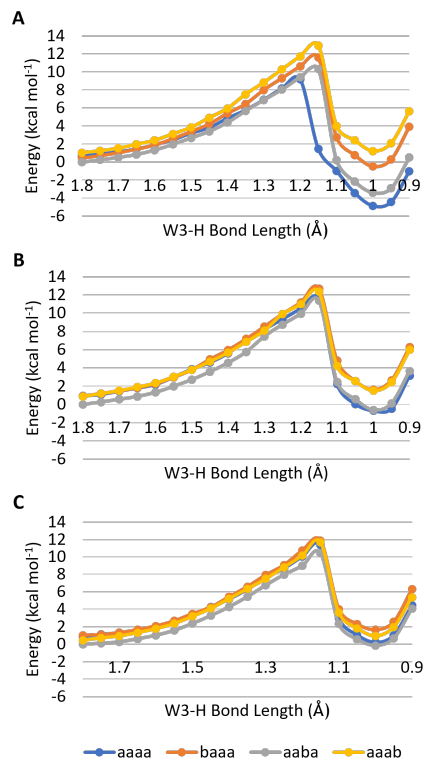
Figure 7: Energy profile of **A**: scan of increasing O6-H$_{O6}$ distance, towards W3, at a fixed **r**[O5O6] = 1.9 Å; **B**: scan of increasing O6-H$_{O6}$ distance, towards W3, at a fixed **r**[O5O6] = 2.0 Å; **C**: scan of decreasing W3-H$_{O6}$ distance, at a fixed **r**[O5O6] = 2.1 Å. Each profile is normalised to their respective HS oxo-hydroxo geometry at **r**[W3-HO6] = 1.8 Å.

3.2. Variation of O5-O6 Separation

It has been shown previously [32] that complete relaxation of the S3 oxo-hydroxo structure results in a geometric minima with an **r**[O5O6] = ≈2.4 Å. To investigate the effect of O5-O6 separation on the deprotonation of O6, additional scans were conducted at a **r**[O5O6] = 1.9 Å and from 2.1 Å to 2.3 Å. Initial scans were carried out by extending the O6-H$_{O6}$ bond; at 1.9 Å and 2.0 Å these scans resulted in proton abstraction by W3 (figure 7; top and middle, respectively), however, at 2.1 Å this approach resulted in an attempted abstraction by Glu189. To address this, an additional scan was conducted by shortening the W3-H$_{O6}$ distance to assess the relevant pathway (figure 7; bottom).

Comparison of the 1.9 Å and 2.0 Å curves show a near identical profile,
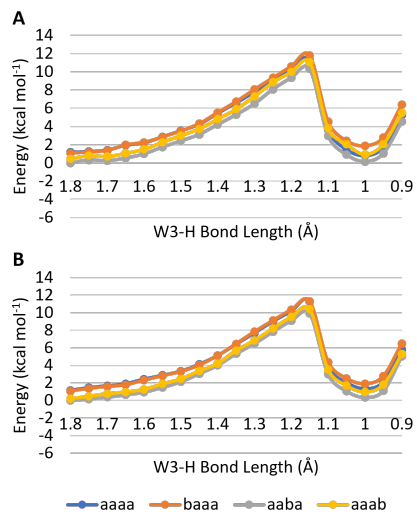
Figure 8: **A**: Energy profile of scan of decreasing W3-H_{O6} distance, at a $\mathbf{r}[O5O6] = 2.2$ Å; **B**: Energy profile of scan of decreasing W3-H_{O6} distance, at a $\mathbf{r}[O5O6] = 2.3$ Å. Each profile is normalised to their respective HS oxo-hydroxo geometry at $\mathbf{r}[W3-HO6] = 1.8$ Å.

with the difference in overall energy explained by the shortening of the O5-O6 distance. The only notable difference in the profiles is the shift of the **aaba** proton rearrangement to coincide with that of the 2.0 Å profile. In contrast, comparison of the 2.0 Å and 2.1 Å surfaces (figure 7; middle and bottom, respectively) shows more significant variation.

The explanation for the relative instability of the oxo-oxo structure, par-

Figure 9: Energy profiles of the high-spin (aaaa) scans over the W3-H distance, at various values of $\mathbf{r}[O5O6]$, such that OO-19 equates to $\mathbf{r}[O5O6] = 1.9$ Å.

11

ticularly in light of the equivalent proton rearrangement barrier (≈ 11 $kcal$ mol^{-1}) can be found in the IBOs (figure S21; top) and the spin distribution of the relevant centres (figu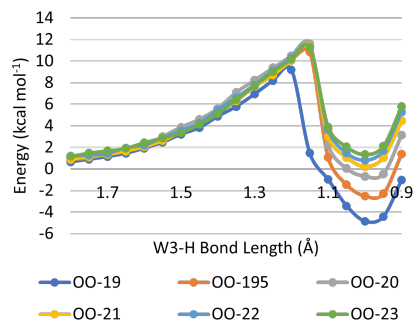re S5). While these data show similar electron movement as observed at the 2.0 Å separation (figure 6) there are notable differences at $\mathbf{r}$[O5O6] = 2.1 Å. Donation of the β electron from the O6 LP into the Mn1 centre (figure 6 & S21; magenta), and an α electron from O5 to Mn4 (figure 6; blue, figure S21; purple) remains comparable, the increase in O5-O6 distance results in significantly lower transfer of the O6 LP α electron from O6 to O5 (figure 6; green, figure S21; blue). This lesser degree of electronic donation from O6 to O5 is evident in the relevant spin held on O6 in the oxo-oxo structure; at 2.0 Å this value is 0.081, compared to a value of 0.135 at 2.1 Å. This effect is also observed, to a similar degree, in the O5 and Mn4 centres, showing values of -0.280 & 3.504 at 2.0 Å compared to the reduced -0.260 & 3.459 at 2.1 Å. That the effect of the increased O5-O6 distance is observed on the O6, O5, and Mn4 centres, serves to further suggest that the donation of the α electron from O6 to Mn4 plays a significant role in the eventual reduction of the Mn4 centre as the reaction progresses.

This observation is further evidenced though consideration of the PES at a 2.2 & 2.3 Å O5-O6 separation (figure 8). At these separations, the trend of relative destabilisation observed from the 2.0 & and 2.1 Å continues with the oxo-oxo structure now being marginally less stable than their equivalent oxo-hydroxo structure by ≈ 1 $kcal$ mol^{-1} (2.2 Å) and ≈ 1.5 $kcal$ mol^{-1} (2.3 Å), directly linking the O5-O6 distance to the stability of the resulting oxo-oxo structure. Despite their energetic differences, the 2.0 & 2.1 Å spin distributions show similar overall trend regarding the Mn4, O5, & O6 centres; however, increasing $\mathbf{r}$[O5O6] from 2.1 Å to 2.2 Å (figure 11) causes a significant change in the the spin distribution, to the point of baring more similarity to the **abaa** & **aaab** distributions at shorter separations (figure 5; bottom). The most significant feature is the sole accumulation of spin on the O6 centre, without any corresponding increase in the spin on O5 or Mn4, further showing that the transfer of spin away from O6 and specifically towards Mn4, is a key factor in oxo-oxo stabilisation.

Across the range of $\mathbf{r}$[O5O6] values presented in this work, the observed trend of a steadily increasing stability of the oxo-oxo structure compared to the oxo-hydroxo starting point is most readily explained by behaviour of the α component of the active O6 lone pair. Considering the IBO representation of this orbital at different values of $\mathbf{r}$[O5O6] (figure 10) shows minimal change in character at the oxo-hydroxo geometry while, in the oxo-oxo struc-
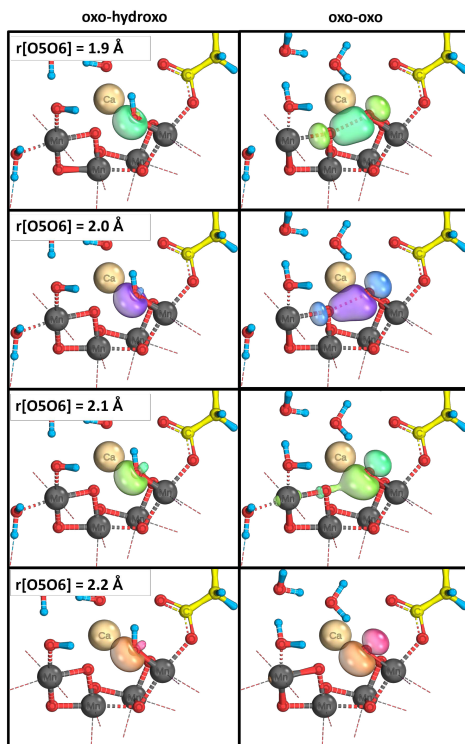
Figure 10: **A**: Plot of IBO changes for the α component of the O6 LP during abstraction by W3 at differing values of **r**[O5O6] in the **aaaa** state; **B**: corresponding IBO representation of the α component of the O6 LP at the oxo-hydroxo (left) and oxo-oxo (right) structures during W3 abstraction.

ture, a steadily increasing orbital change is observed from **r**[O5O6] = 2.1 Å to **r**[O5O6] = 1.9 Å (figure 10; A), forming an overlap with O5 in line with the initiation of a one electron bond (figure 10; B). In contrast, no such overlap is observed at **r**[O5O6] = 2.2 or 2.3 Å; a small degree of orbital distortion is observed in the oxo-oxo structure suggesting the distance is still small enough to allow for interaction between the O5 and O6 centres, but too long to allow for any electron sharing.

A direct comparison of this data should be drawn with similar data put forward by Isobe *et al* [64] based on the 5WS6 crystal structure derived by Suga *et al* [12]. A transition barrier of $\approx$24 *kcal mol*$^{-1}$ is quoted, a significant increase when compared to the barrier presented here. However, the model presented by Isobe *et al* assumes the direct transfer of a proton from W3 to W2; to facilitate this transfer, a substantial rearrangement of both the Mn4

13
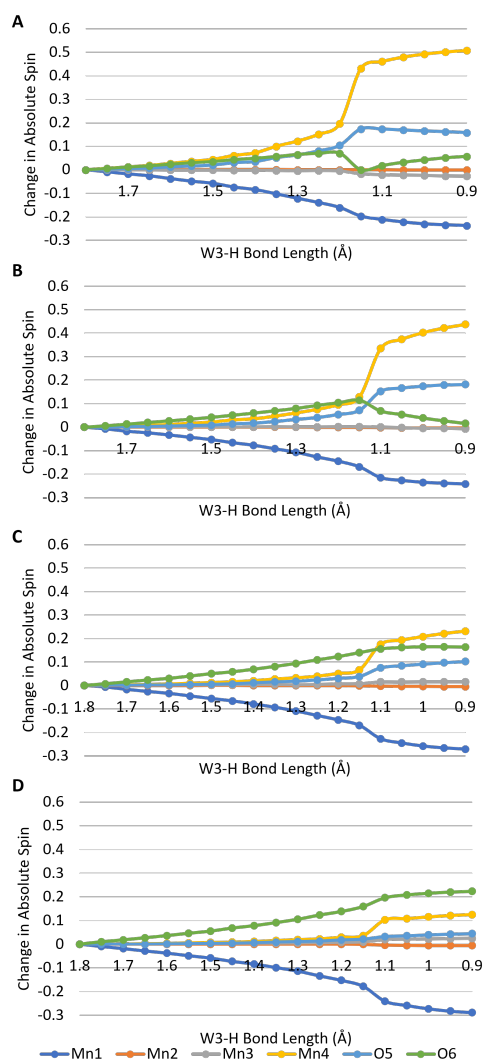
Figure 11: Change in absolute spin values of key atomic centres within the system during the oxo-hydroxo to oxo-oxo transition within the **aaaa** state at $\mathbf{r}$[O5O6] = 1.9 Å (**A**); 2.0 Å (**B**); 2.1 Å (**C**); 2.2 Å (**D**).

and Ca coordination geometries is required, introducing significant strain on the system. In comparison, the presence of a crystallographic water bridging W3 and W2 as found in the 7RF8 structure [22] and by extension, the model presented here, which acts to mitigate the need for that strain and, as a result, lowering the overall barrier for proton rearrangement. Additionally,

14
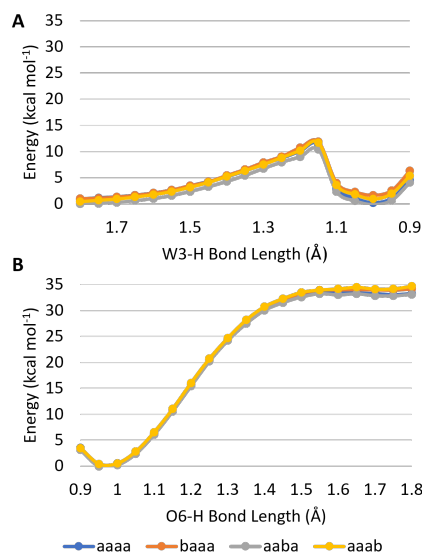
Figure 12: Energy profile of **A**: full scan of increasing W3-H$_{O6}$ distance, at a fixed **r**[O5O6] = 2.1 Å; **B**: scan of increasing O6-H$_{O6}$ distance, towards Glu189, at a fixed **r**[O5O6] = 2.1 Å.

while the transition presented by Isobe *et al* showed a **r**[O5O6] = 2.41 Å this distance, as shown throughout this work would negate any stabilisation from the formation of the one-electron bond between the O5 and O6 centres. In contrast, at the 2.0 Å separation presented here, this stabilisation is not only possible, but is shown to play a central role in the stabilisation of the deprotonated product.

3.3. W3 vs. Glu-189 Abstraction

Given its close proximity to O6, and prevalence in the literature, in order to access the performance of Glu-189 as an alternative proton acceptor, an equivalent analysis was conducted at an **r**[O5O6] = 2.1 Å and 2.2 Å. These separations were chosen due to the observation that, while simply extending the O6-H$_{O6}$ bond at 1.9 & 2.0 Å resulted in abstraction by W3, with no interference from Glu-189, at 2.1 Å lengthening of the O6-H$_{O6}$ bond resulted in attempted abstraction by Glu-189; in contrast, modelling abstraction by W3 required a specific shortening of the W3-H$_{O6}$ distance.

While consideration of the W3 abstraction profile (figure 12; A) shows a clear reaction profile, resulting in the expected split in BS states and a marginally more stable oxo-oxo form when compared to the oxo-hydroxo

15
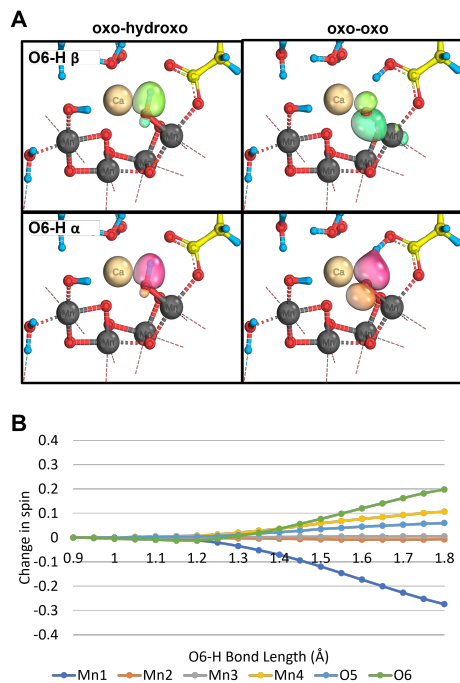
Figure 13: Orbital and spin analysis during Glu189 abstraction in the **aaaa** state at a fixed O5-O6 distance of 2.1Å. **A**: IBO representations of the orbitals showing the largest change over the transition between the oxo-hydroxo (left) and oxo-oxo (right) structures. **B**: The corresponding change in spin distribution with regard to the O5, O6, and Mn centres.

starting point, the profile of the abstraction by Glu-189 presents a stark contrast. Initial consideration of the Glu-189 abstraction profile (figure 12; B) reveals that, not only does stretching the $O6\text{-}H_{O6}$ bond result in an ≈ 33 $kcal\ mol^{-1}$ destabilisation of the complex, but that there is only negligible local minimum to be found with Glu-189 protonated ($\approx 0.5\ kcal\ mol^{-1}$ for the **aaaa** state). Explanation of this significant destabilisation can be rationalised through the IBO and spin data for this particular reaction profile (figure 13; top and bottom, respectively); instead of an O6 lone pair proceeding to interact with the surrounding Mn centres, as seen in the W3 abstraction (figures 6 & S21), the lack of rotation of the $O6\text{-}H_{O6}$ bond away from Glu-189 and towards the calcium prevents the orientation, and resulting overlap necessary to allow for lone pair interaction as the $O6\text{-}H_{O6}$ bond stretches. Instead, figure 13 highlights that it is the β electron of the $O6\text{-}H_{O6}$

16

bond that proceeds to interact with Mn1; in contrast, the α electron from the O6-H$_{O6}$ bond remains localised to the O6 centre, with a significant distortion towards the Glu-189-H$_{O6}$ centre suggesting the maintenance of a significant hydrogen bond character between O6 and H$_{O6}$ which, coupled with the larger electronegativity to be expected on O6 in comparison to the corresponding oxygen on Glu-189, provides insight to the lack of a Glu-189-H$_{O6}$ local minimum, with the pull from O6, held in close proximity to H$_{O6}$ promoting a near barrierless re-abstraction pathway, returning H$_{O6}$ to O6, resulting once again in the vastly more stable oxo-hydroxo structural arrangement.

These data, in which abstraction via Glu189 is highly disfavoured, presents a similar description as that put forward by Mandal *et al*[65]. In addition to the presentation of both spin and orbital analysis (figure 13) to explain the source of the disfavoured energetics, the proposed abstraction via W3 and eventual protonation of W2 results fits into the findings of Mandal *et al* [65] in which, of the ligated water molecules throughout the OEC, the protons of W1 are shown to be the most labile, presenting a minimal transfer barrier between W1 and the local Asp61 residue. These findings, when coupled, further suggest that proton egress may occur through the O4 channel, facilitated though inter-ligand proton transfer from W2 to W1.

Despite the clear energetic preference for abstraction via W3, lengthening of the O6-H$_{O6}$ bond alone did not appear to promote this result. However, this can be explained through analysis of the complete range of the corresponding W3 abstraction profile (figure 12; A); the rotation of the O6-H$_{O6}$ bond to orientate towards W3 is associated with an ≈ 1 *kcal mol*$^{-1}$ barrier before interaction with W3 occurs. While small, this barrier is sufficient to prevent an optimisation from choosing to rotate away from the Glu-189 orientation, akin to opting to remain in the same valley despite the steep climb.

In addition to the strong energetic, and electronic arguments against abstraction by Glu-189, it is also worth considering the structural arguments against this pathway, each of which has a corresponding point of favour in terms of W3 abstraction. These arguments primarily revolve around the idea that in situation in which Glu-189 is protonated, there is no clear and/or obvious pathway through which the deprotonation can occur (omitting O6 as an option) in order to reset Glu-189 before reorientation and re-coordination to the calcium centre during the next catalytic cycle with only two possible pathways presenting themselves. The first of these involves subsequent deprotonation of Glu-189 through W7, onwards to Y$_Z$, and proceeding out through the Y$_Z$ network,[22] for which there is no experimental precedent,

primarily as it would involve the loss of the Y_Z proton, in contrast to the commonly held proton-switch mechanism in which the same proton moves from Y_Z to His-190 and back again depending on the oxidation state of Y_Z. The second pathway involves passing the proton back into the 5-member water wheel[22] for it to then proceed back out through the O1 channel. Both of these options necessitate a substantial reorientation of the Glu-189-H_{O6} bond which presents a significant barrier for the required rotation, in addition to presenting poor interaction with the relevant water molecules that would be required for further proton transfer.

In contrast, abstraction through W3, in addition to the energetic and electronic results, also presents two clear potential routes for eventual expulsion of the proton into the lumen. The first of these, as modelled here, involves a shuffling of protons toward W2 where inter-ligand proton transfer between W2 & W1 provides access to the coordinating Asp residue and subsequently to the O4 channel, as shown by Bhowmick *et al* [66]. Alternatively, should the protonation state of W1 & W2 result in inability for proton acceptance, the conserved crystallographic water modelled here provides a link to the Cl channel which has been strongly argued as a proton transfer route by Hussein *et al*[22].

Each of these structural arguments, relying on well understood features, acts to further bolster the identification of W3 as the preferred proton acceptor when it comes to the final deprotonation of O6.

4. Conclusions and Outlook

A comprehensive analysis of proton abstraction via the Ca-coordinated W3 shows a steady increase in the relative stability of the deprotonated oxo-oxo state with decreasing $\mathbf{r}$[O5O6] separation, when compared to the oxo-hydroxo starting structure. Interpretation of both spin and IBO data across the potential energy surfaces presented throughout this work highlight that the nature of this emerging stability is driven by the ability of O6 to distribute the resulting spin across the Mn1 and O5 centres, preventing an overall accumulation of charge on O6. The distribution of α spin from an O6 lone pair across O5 and Mn4 results in initial formation of a partial O5-O6 bond, while donation of the corresponding β spin to Mn1 acts to stabilise the second electron before formation of the first bond is competed. Interruption of these spin distribution pathways, as observed in the **baaa** & **aaab** states, results in a significant accumulation of spin on the O6 centre and a

18

corresponding reduction in stabilisation when compared to the oxo-hydroxo equivalent.

Similar analysis of abstraction via Glu189 provides significant evidence against the prevalence of this pathway with no stable oxo-oxo minima observed. Instead, the lack of rotation around the O6-Mn1 bond results in the active electrons coming instead from the O6-H$_{O6}$ bond; additionally, while donation of the β electron towards Mn1 still occurs, the formation of a hydrogen bond from the newly protonated Glu189 back to O6 results in reduced movement of α electron required for O5-O6 bond formation.

Overall, this work presents a strong case for both proton abstraction via W3, in addition to the emergence of an oxo-oxo electronic arrangement as a result of the final O6 deprotonation event. Despite the close proximity, and optimal hydrogen-bond orientation, of Glu189 in a wide range of modern crystal structures, we are able to demonstrate, and provide reasoning, for this residue being an inviable proton acceptor within the S3 state, failing to reproduce the relevant electronic arrangement, or a route for proton egress from the OEC.

References

[1] B. Kok, B. Forbush, M. McGloin, Cooperation of charges in photosynthetic O$_2$ evolution–I. a linear four step mechanism, Photochemistry and Photobiology 11 (6) (1970) 457–475.

[2] H. Dau, E. Fujita, L. Sun, Artificial photosynthesis: Beyond mimicking nature, ChemSusChem 10 (22) (2017) 4228–4235.

[3] N. Cox, D. A. Pantazis, F. Neese, W. Lubitz, Artifical photosynthesis: Understanding water splitting in nature, Interface Focus 5 (2015) 20150009.

[4] T. A. Faunce, W. Lubitz, A. W. Rutherford, D. R. MacFarlane, G. F. Moore, P. Yang, D. G. Nocera, T. A. Moore, D. H. Gregory, F. S., K. B. Yoon, F. A. Armstrong, M. R. Wasielewski, S. Styring, Energy and environment policy case for a global project on artificial photosynthesis, Energy Envirn. Sci. 6 (2013) 695–698.

[5] M. Gratzel, Solar energy conversion by dye-sensitised photovoltaic cells, Inorg. Chem. 44 (2005) 6841–6851.

[6] V. Krewald, M. Retegan, N. Cox, J. Messinger, W. Lubitz, S. De Beer, F. Neese, D. A. Pantazis, Metal oxidation states in biological water splitting, Chem. Sci. 6 (2015) 1676–1695.

[7] V. Krewald, M. Retegan, F. Neese, W. Lubitz, D. A. Pantazis, N. Cox, Spin state as a marker for the structural evolution of nature's water splitting catalyst, Inorg. Chem. 55 (2016) 488–501.

[8] I. Zaharieva, P. Chernev, G. Berggren, M. Anderlund, S. Styring, H. Dau, M. Haumann, Room-temperature energy-sampling Kβ X-ray emission spectroscopy of the Mn_4Ca complex of photosynthesis reveals three manganese-centered oxidation steps and suggests a coordination change prior to O_2 formation, Biochemistry 55 (2016) 4197–4211.

[9] I. Zaharieva, H. Dau, M. Haumann, Room-temperature energy-sampling Kβ X-ray emission spectroscopy of the Mn_4Ca complex of photosynthesis reveals three manganese-centered oxidation steps and suggests a coordination change prior to O_2 formation, Biochemistry 55 (2016) 6996–7004.

[10] J. Kern, R. Chatterjee, I. D. Young, F. D. Fuller, L. Lassalle, M. Ibrahim, S. Gul, T. Fransson, A. S. Brewster, R. Alonso-Mori, R. Hussein, M. Zhang, L. Douthit, C. de Lichtenberg, C. M. H., D. Shevela, J. Wersig, I. Seuffert, D. Sokaras, E. Pastor, C. Weninger, T. Kroll, R. G. Sierra, P. Aller, A. Butryn, A. M. Orville, M. Liang, A. Batyuk, J. E. Koglin, S. Carbajo, S. Boutet, N. W. Moriarty, J. M. Holton, H. Dobbek, P. D. Adams, U. Bergmann, N. K. Sauter, A. Zouni, J. Messinger, J. Yano, V. K. Yachandra, Structures of the intermediates of kok's photosynthetic water oxidation clock, Nature 563 (2018) 421–425.

[11] M. Suga, F. Akita, K. Yamashita, Y. Nakajima, G. Ueno, H. Li, T. Yamane, K. Hirata, Y. Umena, S. Yonekura, L. Yu, H. Murakami, T. Nomura, T. Kimura, M. Kubo, S. Baba, T. Kumasaka, K. Tono, M. Yabashi, H. Isobe, K. Yamaguchi, M. Yamamoto, H. Ago, J. Shen, Electronic structure of the oxygen-evolving complex in photosystem II prior to O-O bond formation, Science 345 (2014) 804–808.

[12] M. Suga, F. Akita, M. Sugahara, M. Kubo, Y. Nakajima, T. Nakane, K. Yamashita, Y. Umena, M. Nakabayashi, T. Yamane, N. T.,

M. Suzuki, T. Masuda, S. Inone, T. Kimura, T. Nomura, S. Yonejura, L. Yu, T. Sakamoto, T. Motomura, J. Chen, Y. Kato, T. Noguchi, K. Tono, Y. Joti, T. Kameshima, T. Hatsui, E. Nango, R. Tanaka, H. Naitow, Y. Matsuura, A. Yamashita, M. Yamamoto, O. Nureki, M. Yabashi, T. Ishikawa, S. Iwata, J. Shen, Light-induced structural changes and the site of O=O bond formation in PSII caught by XFEL, Nature 543 (2017) 131–135.

[13] F. Rummel, P. J. O'Malley, How nature makes O_2: an electronic level mechanism for water oxidation in photosynthesis, The Journal of Physical Chemistry B 126 (41) (2022) 8214–8221.

[14] T. A. Corry, P. J. O'Malley, Evidence of O–O bond formation in the final metastable S_3 state of nature's water oxidizing complex implying a novel mechanism of water oxidation, The Journal of Physical Chemistry Letters 9 (21) (2018) 6269–6274.

[15] T. A. Betley, Y. Surendranath, M. V. Childress, G. E. Alliger, R. Fu, C. C. Cummins, D. G. Nocera, A ligand field chemistry of oxygen generation by the oxygen-evolving complex and synthetic active sites, Philosophical Transactions of the Royal Society B: Biological Sciences 363 (1494) (2008) 1293–1303.

[16] T. Saito, S. Yamanaka, K. Kanda, H. Isobe, Y. Takano, Y. Shigeta, Y. Umena, K. Kawakami, J.-R. Shen, N. Kamiya, M. Okumura, M. Shoji, Y. Yoshioka, K. Yamaguchi, Possible mechanisms of water splitting reaction based on proton and electron release pathways revealed for $CaMn_4O_5$ cluster of PSII refined to 1.9 Å X-ray resolution, International Journal of Quantum Chemistry 112 (1) (2012) 253–276.

[17] D. J. Vinyard, S. Khan, G. W. Brudvig, Photosynthetic water oxidation: binding and activation of substrate waters for O–O bond formation, Faraday Discuss. 185 (2015) 37–50.

[18] V. Krewald, F. Neese, D. A. Pantazis, Implications of structural heterogeneity for the electronic structure of the final oxygen-evolving intermediate in photosystem II, Journal of Inorganic Biochemistry 199 (2019) 110797.

[19] T. A. Corry, P. J. O'Malley, Electronic–level view of O–O bond formation in nature's water oxidizing complex, The Journal of Physical Chemistry Letters 11 (10) (2020) 4221–4225.

[20] T. A. Corry, P. J. O'Malley, Evidence of O–O bond formation in the final metastable S_3 state of nature's water oxidizing complex implying a novel mechanism of water oxidation, The Journal of Physical Chemistry Letters 9 (21) (2018) 6269–6274.

[21] P. E. Siegbahn, Water oxidation mechanism in photosystem II, including oxidations, proton release pathways, O—O bond formation and O_2 release, Biochimica et Biophysica Acta (BBA) - Bioenergetics 1827 (8) (2013) 1003–1019.

[22] R. Hussein, M. Ibrahim, A. Bhowmick, P. S. Simon, R. Chatterjee, L. Lassalle, M. D. Doyle, I. Bogacz, I. Kim, M. H. Cheah, S. Gul, C. de Lichtenberg, P. Chernev, C. C. Pham, I. D. Young, S. Carbajo, F. D. Fuller, R. Alonso-Mori, A. Batyuk, K. D. Sutherlin, A. S. Brewster, R. Bolotovski, D. Mendez, J. M. Holton, N. W. Moriarty, P. D. Adams, U. Bergmann, N. K. Sauter, H. Dobbek, A. Messinger, J. Zouni, J. Kern, V. K. Yachandra, J. Yano, Structural dynamics in the water and proton channels of photosystem II during the S_2 to S_3 transition, Nat. Commun. 12 (2021) 6531.

[23] M. Ibrahim, T. Fransson, R. Chatterjee, M. H. Cheah, R. Hussein, L. Lassalle, K. D. Sutherlin, I. D. Young, F. D. Fuller, S. Gul, I.-S. Kim, P. S. Simon, C. de Lichtenberg, P. Chernev, I. Bogacz, C. C. Pham, A. M. Orville, N. Saichek, T. Northen, A. Batyuk, S. Carbajo, R. Alonso-Mori, K. Tono, S. Owada, A. Bhowmick, R. Bolotovsky, D. Mendez, N. W. Moriarty, J. M. Holton, H. Dobbek, A. S. Brewster, P. D. Adams, N. K. Sauter, U. Bergmann, A. Zouni, J. Messinger, J. Kern, V. K. Yachandra, J. Yano, Untangling the sequence of events during the S_2 & S_3 transition in photosystem II and implications for the water oxidation mechanism, Proceedings of the National Academy of Sciences 117 (23) (2020) 12624–12635.

[24] N. Cox, D. A. Pantazis, F. Neese, W. Lubitz, Biological water oxidation, Accounts of Chemical Research 46 (7) (2013) 1588–1596.

[25] M. Askerka, G. W. Brudvig, V. S. Batista, The O_2-evolving complex of photosystem II: Recent insights from quantum mechanics/molecular mechanics (QM/MM), extended X-ray absorption fine structure (EXAFS), and femtosecond X-ray crystallography data, Accounts of Chemical Research 50 (1) (2017) 41–48.

[26] H. Kuroda, K. Kawashima, K. Ueda, T. Ikeda, K. Saito, R. Ninomiya, C. Hida, Y. Takahashi, H. Ishikita, Proton transfer pathway from the oxygen-evolving complex in photosystem II substantiated by extensive mutagenesis, Biochimica et Biophysica Acta (BBA) - Bioenergetics 1862 (1) (2021) 148329.

[27] M. Mandal, K. Saito, H. Ishikita, The nature of the short oxygen–oxygen distance in the Mn_4CaO_6 complex of photosystem II crystals, The Journal of Physical Chemistry Letters 11 (23) (2020) 10262–10268.

[28] K. R. Yang, K. V. Lakshmi, G. W. Brudvig, V. S. Batista, Is deprotonation of the oxygen-evolving complex of photosystem II during the S_1 $\rightarrow S_2$ transition suppressed by proton quantum delocalization?, Journal of the American Chemical Society 143 (22) (2021) 8324–8332.

[29] D. Narzi, D. Bovi, L. Guidoni, Pathway for Mn-cluster oxidation by tyrosine-Z in the S_2 state of photosystem II, Proceedings of the National Academy of Sciences 111 (24) (2014) 8723–8728.

[30] K. Kawashima, T. Takaoka, H. Kimura, K. Saito, H. Ishikita, O_2 evolution and recovery of the water-oxidizing enzyme, Nature Communications 9 (1) (2018) 1247.

[31] T. A. Corry, F. Rummel, P. J. O'Malley, Bonding and magnetic exchange pathways in nature's water-oxidizing complex, The Journal of Physical Chemistry B 125 (26) (2021) 7147–7154.

[32] F. Rummel, P. J. O'Malley, How nature makes O_2: an electronic level mechanism for water oxidation in photosynthesis, The Journal of Physical Chemistry B 126 (41) (2022) 8214–8221.

[33] T. A. Corry, P. J. O'Malley, Evidence of O–O bond formation in the final metastable S_3 state of nature's water oxidizing complex implying a novel mechanism of water oxidation, The Journal of Physical Chemistry Letters 9 (21) (2018) 6269–6274.

[34] F. Neese, Software update: the ORCA program system, version 4.0, WIREs Computational Molecular Science 8 (1) (2018) e1327.

[35] B. Miehlich, A. Savin, H. Stoll, H. Preuss, Results obtained with the correlation energy density functionals of Becke and Lee, Yang and Parr, Chem. Phys. Lett. 157 (1989) 200.

[36] C. Lee, W. Yang, R. G. Parr, Development of the Colle-Salvetti correlation-energy formula into a functional of the electron density, Phys. Rev. B 37 (1988) 785.

[37] A. D. Becke, A new mixing of hartree–fock and local density-functional theories, J. Chem. Phys. 98 (1993) 1372.

[38] A. D. Becke, Density-functional exchange-energy approximation with correct asymptotic behavior, Phys. Rev. 38 (1988) 3098.

[39] E. v. Lenthe, E. J. Baerends, J. G. Snijders, Relativistic regular two-component hamiltonians, The Journal of Chemical Physics 99 (6) (1993) 4597–4610.

[40] E. van Lenthe, E. J. Baerends, J. G. Snijders, Relativistic total energy using regular approximations, The Journal of Chemical Physics 101 (11) (1994) 9783–9792.

[41] C. van Wüllen, Molecular density functional calculations in the regular relativistic approximation: Method, application to coinage metal diatomics, hydrides, fluorides and chlorides, and comparison with first-order relativistic calculations, The Journal of Chemical Physics 109 (2) (1998) 392–399.

[42] F. Weigend, R. Ahlrichs, Balanced basis sets of split valence, triple zeta valence and quadruple zeta valence quality for H to Rn: Design and assessment of accuracy, Phys. Chem. Chem. Phys. 7 (2005) 3297–3305.

[43] P. E. M. Siegbahn, Nucleophilic water attack is not a possible mechanism for O–O bond formation in photosystem II, Proceedings of the National Academy of Sciences 114 (19) (2017) 4966–4968.

[44] A. Altun, J. Breidung, F. Neese, W. Thiel, Correlated ab initio and density functional studies on H_2 activation by FeO^+, Journal of Chemical Theory and Computation 10 (9) (2014) 3807–3820.

[45] K. Eichkorn, O. Treutler, H. Öhm, M. Häser, R. Ahlrichs, Auxiliary basis sets to approximate Coulomb potentials, Chemical Physics Letters 240 (4) (1995) 283–290.

[46] K. Eichkorn, F. Weigend, O. Treutler, R. Ahlrichs, Auxiliary basis sets for main row atoms and transition metals and their use to approximate Coulomb potentials, Theoretical Chemistry Accounts 97 (1) (1997) 119–124.

[47] F. Weigend, Accurate Coulomb-fitting basis sets for H to Rn, Phys. Chem. Chem. Phys. 8 (2006) 1057–1065.

[48] V. N. Staroverov, G. E. Scuseria, J. Tao, J. P. Perdew, Comparative assessment of a new nonempirical density functional: Molecules and hydrogen-bonded complexes, The Journal of Chemical Physics 119 (23) (2003) 12129–12137.

[49] F. Neese, F. Wennmohs, A. Hansen, U. Becker, Efficient, approximate and parallel Hartree–Fock and hybrid DFT calculations. a 'chain-of-spheres' algorithm for the Hartree–Fock exchange, Chemical Physics 356 (1) (2009) 98–109.

[50] J. Tomasi, B. Mennucci, R. Cammi, Quantum mechanical continuum solvation models, Chem. Rev. 105 (2005) 2999.

[51] F. Lipparini, G. Scalmani, B. Mennucci, E. Cances, M. Caricato, M. J. Frisch, A variational formulation of the polarizable continuum model, J. Chem. Phys. 133 (2010) 014106.

[52] N. Cox, M. Retegan, F. Neese, D. A. Pantazis, A. Boussac, W. Lubitz, Electronic structure of the oxygen-evolving complex in photosystem II prior to O-O bond formation, Science 345 (6198) (2014) 804–808.

[53] D. A. Pantazis, W. Ames, N. Cox, W. Lubitz, F. Neese, Two inter-convertible structures that explain the spectroscopic properties of the oxygen-evolving complex of photosystem II in the S_2 state, Angewandte Chemie International Edition 51 (39) (2012) 9935–9940.

[54] S. Grimme, S. Ehrlich, L. Goerigk, Effect of the damping function in dispersion corrected density functional theory, J. Comp. Chem. 32 (2011) 1456.

[55] A. D. Becke, E. R. Johnson, Exchange-hole dipole moment and the dispersion interaction revisited, J. Chem. Phys. 127 (2007) 154108.

[56] A. D. Becke, E. R. Johnson, Exchange-hole dipole moment and the dispersion interaction, J. Chem. Phys. 122 (2005) 154104.

[57] A. D. Becke, E. R. Johnson, A density-functional model of the dispersion interaction, J. Chem. Phys. 123 (2005) 154101.

[58] A. D. Becke, E. R. Johnson, A post-hartree-fock model of intermolecular interactions: Inclusion of higher-order corrections, J. Chem. Phys. 124 (2006) 174104.

[59] F. Neese, The ORCA program system, WIREs Computational Molecular Science 2 (1) (2012) 73–78.

[60] G. Knizia, Intrinsic atomic orbitals: An unbiased bridge between quantum theory and chemical concepts, J. Chem. Theory Comput. 9 (2013) 4834–4843.

[61] G. Knizia, J. E. M. N. Klein, Electron flow in reaction mechanisms — revealed from first principles, Angew. Chem. Int. Ed. 54 (2015) 5518–5522.

[62] T. A. Corry, P. J. O'Malley, Electronic–level view of O–O bond formation in nature's water oxidizing complex, The Journal of Physical Chemistry Letters 11 (10) (2020) 4221–4225.

[63] T. A. Corry, P. J. O'Malley, S_3 state models of nature's water oxidizing complex: Analysis of bonding and magnetic exchange pathways, assessment of experimental electron paramagnetic resonance data, and implications for the water oxidation mechanism, The Journal of Physical Chemistry B 125 (36) (2021) 10097–10107.

[64] H. Isobe, M. Shoji, T. Suzuki, J. Shen, K. Yamaguchi, Spin, valence, and structural isomerism in the S_3 state of the oxygen-evolving complex of photosystem II as a manifestation of multimetallic cooperativity, J. Chem. Theory Comput. 15 (2019) 2375–2391.

[65] M. Mandal, K. Saito, H. Ishikita, The nature of the short oxygen-oxygen distance in the Mn_4CaO_6 complex of photosystem ii crystals, J. Phys. Chem. Lett. 11 (2020) 10262–10268.

[66] A. Bhowmick, R. Hussein, I. Bogacz, P. S. Simon, M. Ibrahim, R. Chatterjee, D. Doyle, Margaret, H. Cheah, Mun, T. Fransson, P. Chernev, I. Kim, H. Makita, M. Dasgupta, J. Kaminsky, Corey, M. Zhang, J. Gätcke, S. Haupt, I. Nangca, Isabela, M. Keable, Stephen, O. Aydin, A., K. Tono, S. Owada, B. GEe, Leland, D. Fuller, Franklin, A. Batyuk, R. Alonso-Mori, M. Holton, James, W. Paley, Daniel, W. Moriarty, Nigel, F. Mamedov, D. Adams, Paul, S. Brewster, Aaron, H. Dobbek, K. Sauter, Nicholas, U. Bergmann, A. Zouni, J. Messinger, J. Kern, J. Yano, K. Yachandra, Vittal, Structural evidence for intermediates during O_2 formation in photosystem II, Nature 617 (2023) 629–636.